Influence of Bottom Friction on Sea Surface Roughness and Its Impact on Shallow Water Wind Wave Modeling

HAKEEM K. JOHNSON AND HENRIK KOFOED-HANSEN

Danish Hydraulic Institute, Horsholm, Denmark

(Manuscript received 20 May 1999, in final form 23 August 1999)

ABSTRACT

Using a selected subset of the measured data obtained in shallow waters near Vindeby, Denmark, during RASEX (Risø Air–Sea Experiment), the role of bottom friction dissipation in predicting wind waves (not swell) is assessed with a third-generation numerical wind wave model. The RASEX measurement site is located in relatively shallow waters (depths of about 3 to 4 m) in an area where the waves are predominantly fetch limited (i.e., maximum fetch of about 20 km).

The bottom friction dissipation source term is modeled using the linearized bottom friction formulation. This formulation contains a dissipation coefficient, C_f, which depends on wave and sediment properties. In the numerical investigations, we considered three cases: (i) a constant value for C_f as obtained in the JONSWAP Experiment, (ii) a constant geometric roughness k_N, and (iii) a constant median sediment size, d_{50}. In the latter case, the bed is treated as a mobile bed and the geometric roughness is related to the dimensions of wave-formed ripples, which is calculated using the empirical expressions of Nielsen. These three cases are investigated using (i) the measured surface winds, U_{10} (where Janssen's theory is used to calculate sea roughness and the corresponding wind stress), and (ii) the measured wind friction speeds, u_*.

Numerical investigations for idealized test cases show that bottom friction dissipation keeps the waves young. This results in high values of sea roughness, wind stress, and wind input source term when Janssen's theory for the coupling between waves and wind stress is used. Using the RASEX dataset, it is shown that Janssen's theory gives too high sea roughness in shallow water. A constant Charnock parameter of 0.015 was found to be better for the event with strong winds. In order to obtain a good agreement between measured and calculated significant wave heights, it was found necessary to use a variable bottom dissipation formulation, where the bottom dissipation coefficient depends in a realistic manner on the hydrodynamic and sediment parameters. The mobile bed friction model with $d_{50} = 0.25$ mm gave almost the same results as the constant geometric roughness model with $k_N = 0.04$ m and are both definite improvement over the constant C_f model (JONSWAP friction model), as has been found elsewhere. This approach gave a dissipation coefficient nearly three times the JONSWAP value.

1. Introduction

Detailed modeling of wind waves is commonly performed using third-generation wind wave models, for example, the WAM model of the WAMDI Group (1988). These models were originally developed for oceanic waters and shelf seas. The model concept is today also quite common for application in shallow and finite water depths (see, e.g., Cavaleri and Holthuijsen 1998). The formulations of some of the dominating physical processes are however still based on those used in deep water.

As waves propagate into shallow water, the orbital wave velocities penetrate the water depth, and the source terms due to wave–bottom interaction become important. Furthermore, the deep water source terms are modified because of depth effects. A review of the different wave–bottom interaction processes is given by Shemdin et al. (1978), who consider dissipation due to friction in the turbulent boundary layer, percolation into a porous bottom, motion of a soft bottom, and scattering by bottom irregularities. According to Shemdin et al. (1978) bottom friction is generally dominant when the sediment is composed of fine sand, $d_{50} = 0.1$–0.4 mm or when sand ripples are present. In this case, the low permeability prohibits percolation and granular friction prevents viscous flow behavior (Shemdin et al. 1978). In many practical cases, the bed is composed of fine sand or wave-generated ripples are present [e.g., Dingler and Inman (1976) found this to be true on many continental shelves].

In the past decades, several formulations for bottom friction in spectral wind wave models has emerged in the literature (see, e.g., Luo and Monbaliu 1994). All

Corresponding author address: Henrik Kofoed-Hansen, Danish Hydraulic Institute (DHI), Agern Allé 5, DK-2970, Hørsholm, Denmark.
E-mail: hkh@dhi.dk

formulations can be generalized into an equation for the bottom friction dissipation source term (Weber 1991). This equation contains a dissipation coefficient, C_f, which in general depends on hydrodynamic and sediment properties. Many different expressions for the dissipation coefficient have emerged in the literature. These expressions can be broadly classified into three categories, namely (i) a constant value as found from the JONSWAP experiment (Hasselmann et al. 1973); (ii) expressions based on the drag law turbulent friction model. This can be based on the assumption of a constant friction factor (Hasselmann and Collins 1968; Collins 1972), constant geometric roughness length k_N (Madsen et al. 1988), or constant median bed sediment size d_{50} (Tolman 1994); and (iii) expressions based on the eddy viscosity model (Weber 1991).

Although the JONSWAP friction model does not relate the dissipation coefficient directly to the local hydrodynamic and sediment conditions, it continues to be used in widely available third-generation wind wave models, such as the WAM model. Komen et al. (1994) reported that tests with regional versions of the WAM model using the JONSWAP dissipation coefficient have proved to be adequate for moderate storms. However, they also added that for extreme storm events, the JONSWAP friction model is not adequate, and the dissipation coefficient should depend on the wave field. For example, in a study of a severe depth-limited storm case in the southern North Sea, Bouws and Komen (1983) found that they needed to increase the JONSWAP dissipation coefficient by almost a factor of 2 in order to obtain an ''equilibrium'' solution.

Weber (1991) also investigated the case of a severe depth-limited storm and an extreme swell case in the southern North Sea. She used an eddy viscosity model for the bottom dissipation and proposed the use of a constant geometric roughness value of $k_N = 0.04$ m for wave modeling in that area. For wave simulation during an extreme storm event in the southern North Sea, Weber's model gave dissipation coefficients similar to that found by Bouws and Komen.

An example of using a mobile-bed bottom friction description in a wave model was described by Tolman (1994); see also Graber and Madsen (1988) and Nielsen (1983). Tolman investigated bottom friction dissipation in a number of idealized test cases with wind wave conditions. He found that the dissipation coefficient is fairly constant for many common roughness regimes in the absence of swell. According to Tolman, this explains the relative success of the JONSWAP friction model used in WAM. Furthermore, he found that variations of the friction factor are most dominated by hydrodynamic effects rather than mobile bed effects. Hence, he concluded that this is the reason for the relative success of models using a single predefined roughness (e.g., Madsen et al. 1988; Weber 1991).

Recently, Young and Gorman (1995) have analyzed the spectral decay, which can be attributed to bottom dissipation processes in the case of Southern Ocean swell. Based on data from a field experiment in the Great Australia Bight, Australia, and an inverse modeling technique using the WAM model, they concluded that the bottom dissipation coefficient C_f is not constant, but varies approximately inversely with the wave-induced bed velocity.

It is now generally accepted that the roughness of the ocean surface depends on the sea state, described by the wave spectrum. In shallow water, dissipation due to bottom friction changes the shape of the spectrum and thus, has an influence on the sea roughness and wind stress. This alters the wind input to the growing sea and the total wave energy balance. Although many investigators have looked into the dissipation of wave energy due to bottom friction, there is very little information (to the knowledge of the authors) on the effect of this dissipation on sea roughness and related wind input. This paper attempts to fill this gap.

In this paper, the influence of bottom friction dissipation on sea roughness in shallow water wind wave modeling is investigated in the protected shallow and fetch limited waters near Vindeby, Denmark. The wave conditions at this site are free of swell. Field observations indicate that the bed material consists of fine sand and patches of seaweed (J. Højstrup 1997, private communication). According to Shemdin et al., this implies that bottom friction is the most dominant wave–bottom interaction mechanism, outside of the surf zone. For this study, measurements of surface wind speeds and directions, waves (integral parameters and frequency spectra), and wind friction speeds are available from the RASEX study (see Bathelmie et al. 1994). The first attempt to reproduce the measured wave parameters using a numerical model is described in Johnson et al. (1999). However, this attempt was not quite successful.

The investigation into bottom friction dissipation is carried out using three different expressions for the dissipation coefficient. These are (i) a constant dissipation coefficient as obtained from JONSWAP; (ii) a constant geometric roughness, $k_N = 0.04$ m as proposed by Weber (1991) for the North Sea; and (iii) a mobile-bed roughness model with a predefined mean sediment size. For the last two cases the dissipation coefficient is based on the local hydrodynamic conditions. Furthermore, in case (iii) the geometric roughness is obtained from the dimensions of the wave-formed ripples based on the empirical expressions of Nielsen (1979) originating from field measurements. Janssen's (1989, 1991) theory for the coupling between waves and sea roughness is used to investigate the influence on sea roughness and wind stress.

The investigations are carried out using the Danish Hydraulic Institute (DHI) third-generation wind wave model, MIKE21 OSW3G. The model is based on the numerical integration of the spectral energy balance equation with default source functions as in WAM cycle 4; see Günther et al. (1992) and Komen et al. (1994).

This paper is arranged as follows. In section 2, a brief description of the governing equations for MIKE 21 OSW3G and the relevant source functions is given. This is followed in section 3 by fetch-limited tests in idealized cases, giving some insight into the role of bottom friction in shallow water and its influence on the sea roughness. In section 4, results of studies at the Vindeby site are presented and discussed. Finally in section 5, a summary of the work done and conclusions from the study are presented.

2. Governing equations

The third-generation wind wave model, MIKE21 OSW3G, has been used to calculate the two-dimensional wave energy spectrum in finite depths. The model is based on numerical integration of the spectral energy balance equation

$$\frac{DF}{Dt} = S_{\text{in}} + S_{\text{nl}} + S_{\text{ds}} + S_{\text{bot}}, \tag{1}$$

where $F(f, \theta, x, y, t)$ represents the spectral energy density, f is frequency, θ is direction, x, y are spatial coordinates, and t is time. The left-hand side of (1) describes the wave propagation in time and space using linear theory. The right-hand side represents the superposition of source functions describing various physical phenomena: the wind input S_{in}, nonlinear energy transfer due to four-wave interaction S_{n1}, dissipation due to whitecapping S_{ds} and bottom dissipation S_{bot}. Nonlinear energy redistribution due to three-wave interaction and energy dissipation due to bottom-induced wave breaking is not considered in this study.

The wind input, S_{in}, is based on Janssen's quasi-linear theory of wind wave generation (Janssen 1989, 1991), where the wind friction velocity u_* and sea surface roughness z_0, not only depend on the wind, but also the sea state itself. The nonlinear transfer of energy S_{n1}, through the resonant four-wave interaction, is approximated by the discrete interaction approximation (DIA) originally proposed by Hasselmann et al. (1985). The source function describing the dissipation due to whitecapping is based on the theory of Hasselmann (1974), tuned according to Janssen (1989).

In order to facilitate the discussion of the role of bottom friction in shallow water and its impact on the wind input, an extended description of the source terms for wind input S_{in} and bottom induced dissipation S_{bot} is given below.

a. Wind input

The wind input source term is parameterized following Janssen's formulation and implemented as in WAM cycle 4; see Komen et al. (1994). For a given wind speed and direction, the growth rate of waves of a given frequency and direction depends on the friction velocity u_* and sea roughness z_0.

In principle, if the sea roughness is known or assumed [e.g., the Charnock (1955) parameter $z_{\text{ch}} = gz_0/u_*^2$, may be assumed], the wind friction speed can be estimated using the logarithmic wind profile. Thus, the growth rate of waves due to wind input can be calculated. Assuming a dimensionless sea roughness ($z_{\text{ch}} = gz_0/u_*^2$) of 0.0144, this formulation was shown in Komen et al. (1994) to fit the observations compiled by Plant (1982). Note that the use of a constant Charnock parameter implies that sea roughness is not coupled with the wave spectrum in the comparison with observations shown in Komen et al.

In addition to the parameterization of the wind input source term, Janssen (1991) parameterized the sea roughness in terms of wave induced stress τ_w, which depends on the wave spectrum. This is the mechanism for the coupling of waves and sea roughness, which is investigated in sections 3 and 4.

b. Dissipation due to bottom friction

All formulations for bottom friction dissipation based on linear theory can be generalized into Eq. (2) (Weber 1991):

$$S_{\text{bot}}(f, \theta) = -C_f \frac{k}{\sinh 2kh} F(f, \theta), \tag{2}$$

where C_f is a dissipation coefficient ($= f_w U_{\text{bm}}$), which depends on the hydrodynamic and sediment conditions. Here f_w is the wave friction factor and U_{bm} is the maximum near-bed particle velocity given by

$$U_{\text{bm}} = \left[\int\int 4 \frac{gk}{\sinh 2kh} F(f, \theta)\, df\, d\theta \right]^{1/2}. \tag{3}$$

Three models for the dissipation coefficient C_f are considered in this paper. These are

- a constant dissipation coefficient as found in the JONSWAP experiment for swell waves or by Bouws and Komen (1983) for storm waves. This will be denoted the JONSWAP friction model (JONF).
- a constant geometric roughness lenght k_N, as suggested by Weber (1991). However, instead of using Weber's expression for the dissipation coefficient (which is based on the eddy viscosity model), we calculate the dissipation coefficient as the product of the wave friction factor using the expression of Jonsson (1966) and the bottom orbital velocity given in Eq. (3). This approach will be called the constant roughness friction model (CRL).
- a constant median sediment size d_{50}, in which the bed is modeled as a mobile bed. Tolman (1994) describes a recent example of this approach. However, our approach differs in the details. In this paper, the ripple geometry is calculated using the empirical expressions of Nielsen (1979), which are based on field measurements including irregular waves. The bed roughness

is calculated using the expression given by Swart (1976). Finally, the dissipation coefficient is computed as the product of the wave friction factor and the bottom orbital velocity, Eq. (3). This approach will be called the mobile-bed friction model (MBF).

The calculation procedure for the wave friction factor and the mobile bed roughness is outlined in the appendix.

c. Numerical integration of the spectral energy balance equation

The integration of the spectral energy balance equation (1) is divided into two steps, namely, a propagation step and a source function integration step. The propagation step is solved using either a semi-Lagrangian scheme described by Brink-Kjaer et al. (1984) or using a first-order upwind scheme (as originally used in the WAM model). In this paper, the first-order scheme is used only. The source integration step is carried out using the method suggested by Komen et al. (1994), see also Hersbach (1998). Details about the numerical model are given in Johnson and Kofoed-Hansen (1998) and are not repeated here.

3. Idealized test cases

In this section we consider a simple idealized test case where the water depth is constant. This makes it easier to focus on the influence of bottom friction on wave growth and sea roughness. This approach was introduced by Komen et al. (1984) in case of fetch-limited wave growth in deep water. Later Weber (1988) studied the spectral energy balance in case of finite depth waves. A constant value of the bottom dissipation ($C_f = 0.0076$ m s^{-1}: Bouws and Komen 1983) was used.

First, we investigate wave growth in deep water and show that model predictions for integral wave parameters (dimensionless H_{m0}, T_p vs fetch) and air–sea parameters (z_0/σ, gz_0/u_*^2 vs u_*/c_p, where $\sigma = \frac{1}{4}H_{m0}$) are consistent with empirical formulas based on field data. Then, we investigate wave growth in shallow water using the three different formulations for bottom friction outlined above. For the shallow water case, it is shown that the bottom friction keeps the waves young, thus increasing the dimensionless sea roughness and the wind input.

The simulations are carried out to cover a fetch range of 1–380 km using two bathymetries. The coarse grid bathymetry has a maximum fetch of 380 km with a grid spacing of 20 km while the fine grid bathymetry has a maximum fetch of 24 km with a grid spacing of 1 km. In both cases the spectrum is resolved by 28 logarithmic-distributed discrete frequencies and 12 evenly spaced directions.

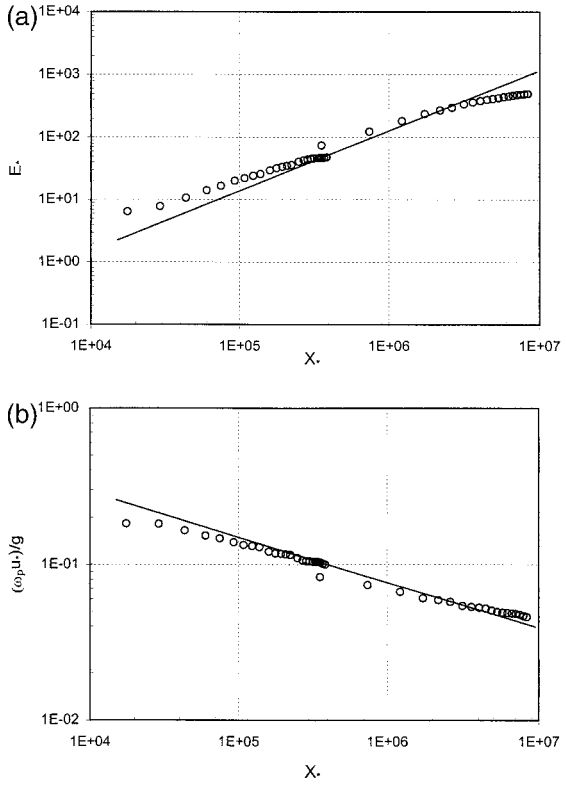

FIG. 1. Comparison between simulated wave parameters (open circles) in deep water and the empirical growth curve of Kahma and Calkoen (1994), (solid line): (a) dimensionless wave energy (g^2E/u_*^4) and (b) dimensionless peak angular frequency ($\omega_p u_*/g$).

a. Wave growth in deep water

The wind speed is constant $U_{10} = 15$ m s^{-1} blowing offshore in the direction of increasing fetch and the sea roughness is calculated using Janssen's theory.

The calculated integral wave parameters and sea roughness are made dimensionless using the calculated wind friction speeds. Figure 1 shows a comparison between the calculated evolution of dimensionless energy and peak angular frequency with the empirical formula of Kahma and Calkoen's (1994) Eqs. (2.226e–f). Note that the data that Kahma and Calkoen used is valid in the range $10^4 < X_* < 4 \times 10^6$. The agreement is, in general, good. However, at small dimensionless fetches ($X_* < 10^5$), the wave model overestimate the wave energy compared to the empirical formula of Kahma and Calkoen. The reason for the discontinuity between the results of the larger (20 km) and the smaller (1 km) resolution runs at $X_* \sim 3.5 \times 10^5$ is due to the change in spatial resolution.

Similarly, a comparison between the calculated dimensionless sea roughness gz_0/u_*^2 (i.e., Charnock parameter, z_{ch}) and the empirical expressions of Johnson et al. (1998) and Smith et al. (1992) is shown in Fig. 2a. The model calculations compare fairly well with both expressions. Good agreement is also obtained when

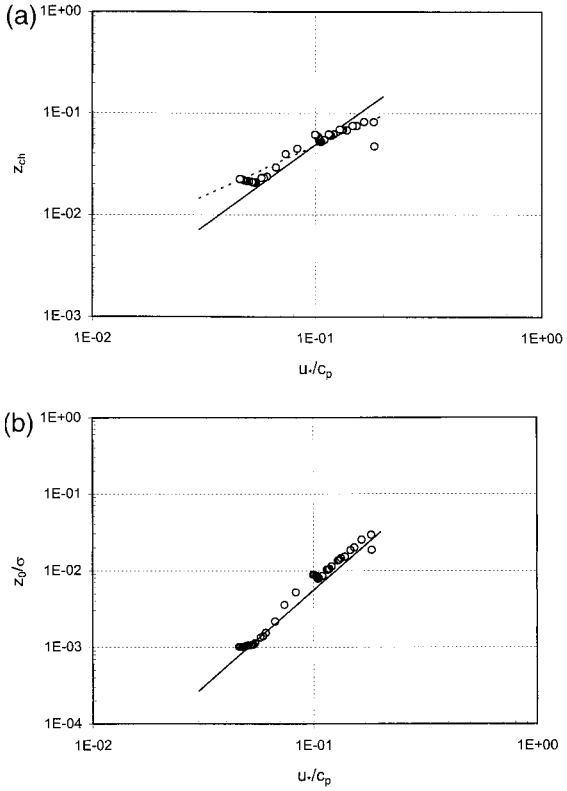

FIG. 2. Comparison between simulated air–sea parameters (open circles) in deep water and empirical formulas: (a) sea roughness scaled with u_* (Charnock parameter, gz_0/u_*^2), (dotted) Johnson et al. (1998) and (solid) Smith et al. (1992); and (b) sea roughness scaled with square root of the variance of the wave spectrum (z_0/σ), (solid) Donelan et al. (1993).

the simulated z_0/σ is compared with the empirical formula suggested by Donelan et al. (1993) in Fig. 2b.

b. Wave growth in shallow water

The shallow water simulations are carried out with a water depth of 15 m. As in the deep water simulations, the wind speed is 15 m s^{-1}, blowing in the direction of increasing fetch. Six simulations corresponding to different descriptions of bottom friction and sea roughness

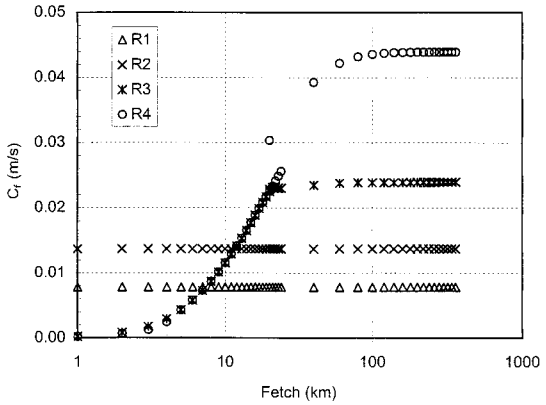

FIG. 3. Variation of bottom dissipation coefficient C_f with fetch using Janssen's theory (R1: JONF ($C_f = 0.0078$ m s^{-1}); R2: JONF ($C_f = 0.0137$ m s^{-1}); R3: CRL ($k_N = 0.04$ m); R4: MBF ($d_{50} = 0.25$ mm).

were carried out. A summary of the settings used for the different simulations is given in Table 1.

The calculated dissipation coefficient versus the fetch is shown in Fig. 3 for the simulations R1, R2, R3, and R4. For simulations R3 and R4, the bottom dissipation coefficient increases with fetch until the waves become depth-limited, whereafter the dissipation coefficient becomes constant. This clearly shows that the assumption of a constant dissipation coefficient is not valid in growing waves as Young and Gorman (1995) found in case of swell. However, in depth-limited conditions, it is sufficient to use a constant dissipation coefficient. Another feature of Fig. 3 is that the dissipation coefficient at equilibrium conditions is considerable higher for R3 (CRL) and R4 (MBF) than the constant values of dissipation coefficient obtained in JONSWAP (R1, $C_f = 0.0077$ m s^{-1}) or by Bouws and Komen (R2, $C_f = 0.013$ m s^{-1}). We remark at this stage that the dissipation coefficient calculated using the MBF module is not always higher than these constant values. In fact, for very strong winds, the ripples at the bed are washed out (due to very high dimensionless bed shear stress), leading to a reduction in the bed roughness and the bottom dissipation coefficient. The apparent agreement between the mobile bed roughness model (R4) and the constant

TABLE 1. Identification of shallow water simulations.

Simulation	Bottom friction description	Method of calculating sea roughness
R0	No bottom friction	Janssen theory
R1	JONF, $C_f = 0.0078$ m s^{-1} (JONSWAP, swell waves)	Janssen theory
R2	JONF, $C_f = 0.0137$ m s^{-1} (Bouws and Komen 1982), wind waves	Janssen theory
R3	CRL, $k_N = 0.04$ m	Janssen theory
R4	MBF, $d_{50} = 0.25$ mm	Janssen theory
R5	MBF, $d_{50} = 0.25$ mm	Charnock formula, $z_{ch} = 0.0185$
R6	JONF, $C_f = 0.0078$ m s^{-1}	Charnock formula, $z_{ch} = 0.0185$

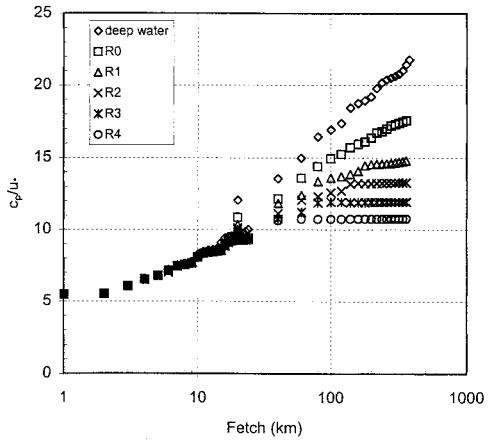

FIG. 4. Variation of wave age (c_p/u_*) with fetch using Janssen's sea roughness theory and different bottom friction formulations (R1: JONF (C_f = 0.0078 m s^{-1}); R2: JONF (C_f = 0.0137 m s^{-1}); R3: CRL (k_N = 0.04 m); R4: MBF (d_{50} = 0.25 mm).

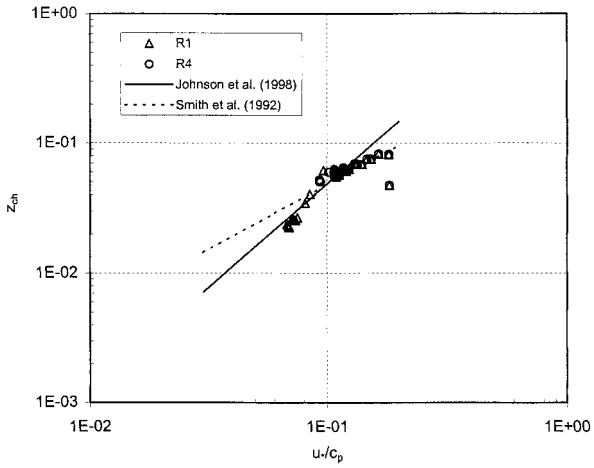

FIG. 5. Comparison between recent empirical formulas and the simulated Charnock parameter (gz_0/u_*^2) using Janssen's sea roughness theory. (R1: JONF (C_f = 0.0078 m s^{-1}); R4: MBF (d_{50} = 0.25 mm).

roughness length model (R3) is because the wave friction factor does not depend on the geometric roughness for the smaller fetch; cf. Eq. (A1).

Now, we investigate the variation of wave age due to bottom friction. Figure 4 shows the variation of wave age (c_p/u_*) with fetch. This figure shows that a reduction of the water depth or increase in bottom friction keeps the wave young. This is caused by two factors: (i) the reduced celerity of wave propagation and (ii) the increase of the peak frequency due to energy dissipation by bottom friction in the forward face of the spectrum. Thus, as the amount of bottom friction increases, waves in shallow water are forced to be young.

Figure 5 shows a plot of the Charnock parameter z_{ch} versus the inverse wave age for simulation R1 (JONF, C_f = 0.0078 m s^{-1}) and R4 (MBF, d_{50} = 0.25 mm). The comparison with the empirical formula of Johnson et al. (1998) looks quite good. A similar comparison using z_0/σ and the empirical results of Donelan et al. (1993) is also good (not shown here). As the waves become depth-limited and the wave age becomes practically constant, as shown in Fig. 4, the corresponding Charnock parameter also becomes practically constant, although at a higher value compared to if the waves are unaffected by bottom friction. Hence, since young waves give high sea roughness, bottom friction according to this theory lead to increase in the wind friction speeds, Fig. 6.

In the next section, we investigate the effects of bottom dissipation using field measurements obtained in the shallow waters near Vindeby, Denmark.

4. Vindeby test case

a. The dataset

The measured data originates from the RASEX measurements, which took place at an offshore wind turbine site near Vindeby, Denmark, in a spring and a fall campaign in 1994. The measurement location is indicated in Fig. 7. Barthelmie et al. (1994) described in detail the instrumentation at the site. The measured data has also been described in some detail by Johnson et al. (1998). Here, a brief description is given.

The experiment comprises two 48-m offshore towers (SMW and SMS in Fig. 7) and one tower on the coast on the island of Lolland. The SMW tower is used for the wind stress measurements. SMW was situated in about 4-m water depth with a 15–20 km upstream fetch in a 90 degree sector with upstream water depths of 5–20 m.

The wind friction velocity was derived from the lowest sonic anemometer (Solent, three-component research type) mounted on SMW at 3 m MSL. Data were logged as 30-min time series with a sampling frequency of 20 Hz. The total wind stress is obtained as:

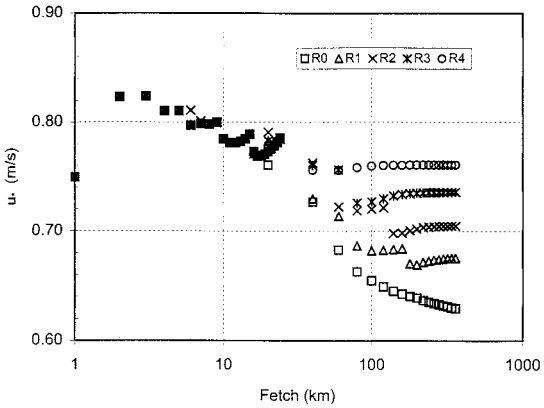

FIG. 6. Variation of wind friction speed u_* with fetch using Janssen's sea roughness theory and different bottom friction formulations (R0: No bottom friction; R1: JONF (C_f = 0.0078 m s^{-1}); R2: JONF (C_f = 0.0137 m s^{-1}); R3: CRL (k_N = 0.04 m); R4: MBF (d_{50} = 0.25 mm).

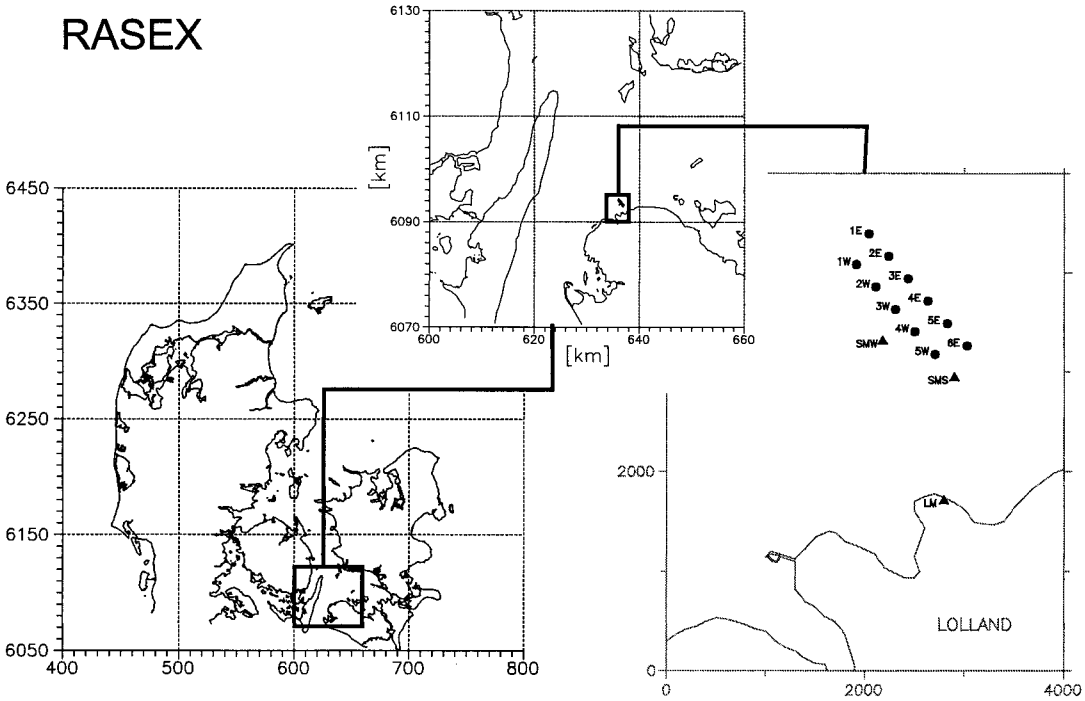

FIG. 7. The RASEX site at Vindeby. From left to right: Denmark—Langeland/Lolland—closeup of site. The filled circles indicate wind turbines, the triangles are the two 48-m offshore lattice towers and the coast tower. The tower used for this study was situated west of the wind farm (SMW). Distances on the two leftmost figures are in kilometers; on the closeup in meters.

$$u^2_* = \sqrt{(\langle uw\rangle^2 + \langle vw\rangle^2)},$$

where $\langle uw\rangle$ and $\langle vw\rangle$ is the along-wind stress and stress perpendicular to mean wind, respectively.

In this paper, we use the mean wind speed measured at an elevation of 7 m MSL on the SMW tower using a cup anemometer. The estimated accuracy is about 2%. The U_{10} wind was obtained from the U_7 wind using the 1/7 power law.

An acoustic wave recorder (AWR) was placed on the sea bottom, about 30 m WNW from the SMW tower. The AWR measured the surface elevations with a sampling frequency of 8 Hz. Spectral analyses were performed on 30-min time series with a cutoff frequency of 2 Hz. From the frequency spectra, characteristic integral measures were derived. These are mean wave periods T_{01} and T_{02} and peak period T_p. The mean wave periods T_{01} $(=m_0/m_1)$, T_{02} $(=\sqrt{m_0/m_2})$ are obtained from the moments of the spectrum, where m_n is the nth spectral moment given by $m_n = \int f^n F(f)\, df$. The peak period is obtained from T_{50} (wave period at which 50% of the variance in the spectrum is found on either side of the frequency $1/T_{50}$) using the relationship between T_p and T_{50} for a standard JONSWAP spectrum with a peak enhancement factor of 1.0 ($T_p = 1.156T_{50}$). This is justified since such a JONSWAP spectrum fits the measured spectra quite well. The significant wave height, H_{m0}, is calculated as four times the standard deviation of the water surface elevations.

b. Model setup

The digitized bathymetry is shown in Fig. 8. A grid spacing of 1 km was used in the horizontal plane. The origin of the grid is at 54.750°N, 10.735°E.

As for the idealized test cases 28 discrete frequencies were chosen with a logarithmic frequency distribution ($f_{n+1} = 1.1 f_n$). The minimum frequency is 0.1 Hz. The number of discrete directions is 12. The propagation time step is chosen as 60 s, while the source time step is selected as 30 s.

Two events were selected from the RASEX dataset and the measured data compared with the numerical model results. The first event is characterized by moderate winds ($U_{10} \approx 10$ m s^{-1}) and the second event by relatively strong winds ($U_{10} \approx 15$ m s^{-1}). The wind conditions during these events are indicated in Fig. 9. For each event, nine simulations corresponding to different descriptions of bottom friction and sea roughness were carried out. A summary of the settings used for the different simulations is given in Table 2. Johnson et al. (1998) found that a constant z_{ch} of 0.018 [which is a typical value for coastal waters; see, e.g., Wu (1980)] was good for predicting the measured wind friction speeds during RASEX. Thus, this value is used for the moderate winds in simulations where the sea roughness is calculated using the Charnock formula (simulation VBR3–VBR8). For the strong winds, a slightly lower value, $z_{ch} = 0.015$, was used, corresponding to

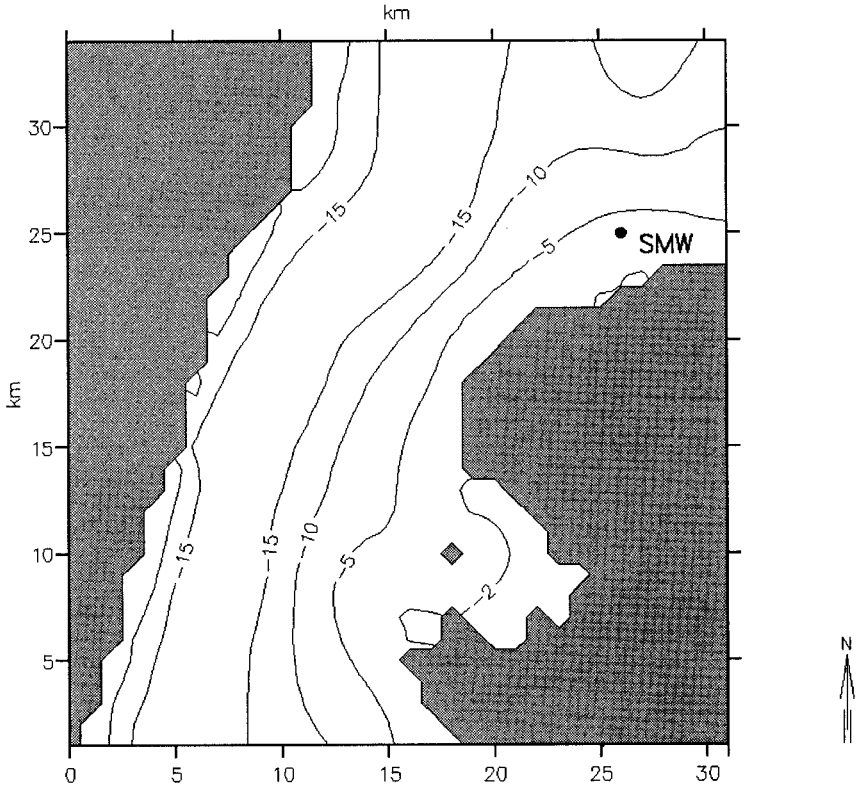

FIG. 8. Digitized bathymetry of the RASEX site at Vindeby. The filled circle indicates the location of the acoustic wave recorder near the SMW tower.

the average z_{ch} derived from measurements during this period.

c. Results of simulations with standard WAM settings

Simulation VBR0 corresponds to the case with standard settings used in our model (as in WAM cycle 4). A comparison between the measured data (significant wave height, peak period, and wind friction velocity) and results from the numerical model for simulation VBR0 is shown in Fig. 10.

It can be seen from Fig. 10 that the wave height, wave period, and wind friction speeds are nearly all overpredicted by the numerical model. For the strong wind event, the overprediction is nearly 100%. However, the overprediction is much less for the moderate wind event.

d. Effect of sea roughness parameterization

The large overprediction of the wave height and period for the strong winds is obviously linked to the overprediction of the wind friction velocity, which goes into the calculation of the source function for wind wave growth. In order to assess the influence of the sea roughness theory on the calculations, integral wave results from simulations VBR3 and VBR6 are compared with the measured data. This comparison is also shown in Fig. 10.

Comparing results from VBR3 and VBR0, some improvement can be seen in the calculated wave parameters. Hence, some of the explanation to the overprediction of the wave climate lies in the computation of the rather high wind friction velocities using Janssen's sea roughness parameterization. These results indicate that a good prediction of u_* is necessary, although not sufficient to give good results.

e. Effect of bottom friction

A comparison between the measured and calculated spectra (for simulation VBR0 and VBR6) at the peak of the storm (1500 local time 1 Nov 1994) during the strong wind event is shown in Fig. 11. Compared to the numerical model results, the measured frequency spectrum indicate significantly more dissipation of low frequency energy than was accounted for by simulations VBR0 and VBR6. Thus, it is logical to investigate the role of bottom friction on the model results. It should here also be noted that the relative wavenumber at the spectral peak is $k_p h \sim 1.5$, that is, well beyond the deep water limit $k_p h \sim 3$.

First, we consider the effect of increasing the constant dissipation coefficient in the JONSWAP bottom friction

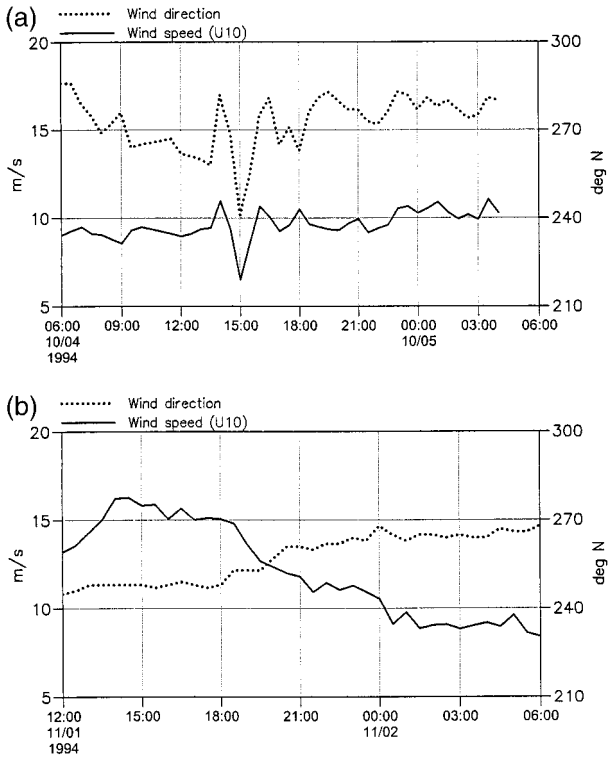

FIG. 9. Wind conditions during periods simulated using the third-generation model MIKE21 OSW3G: (a) event 1 with moderate winds (~10 m s^{-1}), and (b) event 2 with strong winds (~15 m s^{-1}).

TABLE 2. Settings used for the Vindeby simulations.

Simulation	Wind input	Method of calculating sea roughness	Bottom friction description
VBR0	U_{10}	Janssen theory	JONF, C_f = 0.0078 m s^{-1}
VBR1*	U_{10}	Janssen theory	JONF, C_f = 0.0137 m s^{-1}
VBR2*	U_{10}	Janssen theory	JONF, C_f = 0.0233 m s^{-1}
VBR3	U_{10}	Charnock formula	JONF, C_f = 0.0078 m s^{-1}
VBR4	U_{10}	Charnock formula	CRL, k_N = 0.04 m
VBR5*	U_{10}	Charnock formula	MBF, d_{50} = 0.25 mm
VBR6*	u_*	Charnock formula	JONF, C_f = 0.0078 m s^{-1}
VBR7	u_*	Charnock formula	CRL, k_N = 0.04 m
VBR8	u_*	Charnock formula	MBF, d_{50} = 0.25 mm

* Results not shown here.

model (simulations VBR1 and VBR2, not shown here) while using the Janssen's parameterisation for sea roughness. As obtained in section 3 for the idealized test cases, increasing the dissipation coefficient from 0.0078 m s^{-1} (VBR1) to 0.0137 m s^{-1} (VBR2) leads to an increase in the calculated wind friction speeds while the significant wave height and peak period reduces. This result implies that simply increasing the bottom dissipation coefficient makes the difference between the measured and calculated wind friction speeds become larger, although the integral wave parameters is improved somewhat.

As discussed in section 3, the increase in wind friction is due to the waves becoming younger as bottom friction is increased, resulting in increased dimensionless sea roughness. Obviously, this dimensionless sea roughness is too high compared to the measurements. Next, we consider the results using the measured wind friction speeds with sea roughness determined using the Charnock formula and bottom friction calculated using the CRL and MBF formulations (VBR7 and VBR8). A comparison between the measured and calculated wave parameters is shown in Fig. 12. Both VBR7 and VBR8 compares quite well with the measured data. However, a slightly better comparison is obtained with VBR8, which models bottom friction dissipation using the mobile-bed friction module. Similar results are obtained for simulations VBR4 and VBR5 (not shown here), where the U_{10} has been used as input. This is expected as the Charnock parameter has been derived on basis of measured time series of U_{10} and u_*.

Figure 13 shows a time series of the calculated dissipation coefficient (VBR0, VBR7, and VBR8) at the wave measurement location. The bottom dissipation coefficient is on the average about a factor of 3 larger than the empirical JONSWAP value. It is interesting to note that a constant bottom roughness of 0.04 m gives almost the same dissipation coefficient as using the mobile-bed friction module with a median sand size of 0.25 mm. This is due to the presence of wave-formed ripples, which enhances the bed friction. Notice the changes in the dissipation coefficient as the wind speed increases and decreases. This is clearly related to changes in the bottom orbital velocities, since the variation is similar for both VBR7 and VBR8. As can be inferred from this result, additional tests using the wave model indicated that a constant dissipation coefficient does not give good results for both strong winds and moderate winds. Thus, a constant dissipation coefficient cannot adequately reproduce the measured data. A comparison between the measured and calculated spectrum (VBR7 and VBR8) at the peak of the storm is given in Fig. 14. Compared to Fig. 14, the agreement is much improved.

The above results indicate that a reduced wind input (compared to what would have been obtained using Janssen's parameterization for sea roughness) and increased bottom dissipation is required in order to obtain a good comparison between measured and calculated wave parameters in shallow water. It is interesting to note that this result is consistent with the findings of Hersbach (1998), who applied the adjoint of the WAM model to optimize the model parameters required for minimum difference between measured and calculated wave parameters in Lake George, Australia. He found that a reduction in the wind input, reduction in white-capping dissipation and increased bottom dissipation was required to obtain a good comparison between measured and calculated values.

5. Summary and conclusions

The role of bottom friction on wind waves and swell in shallow water has been investigated and examined

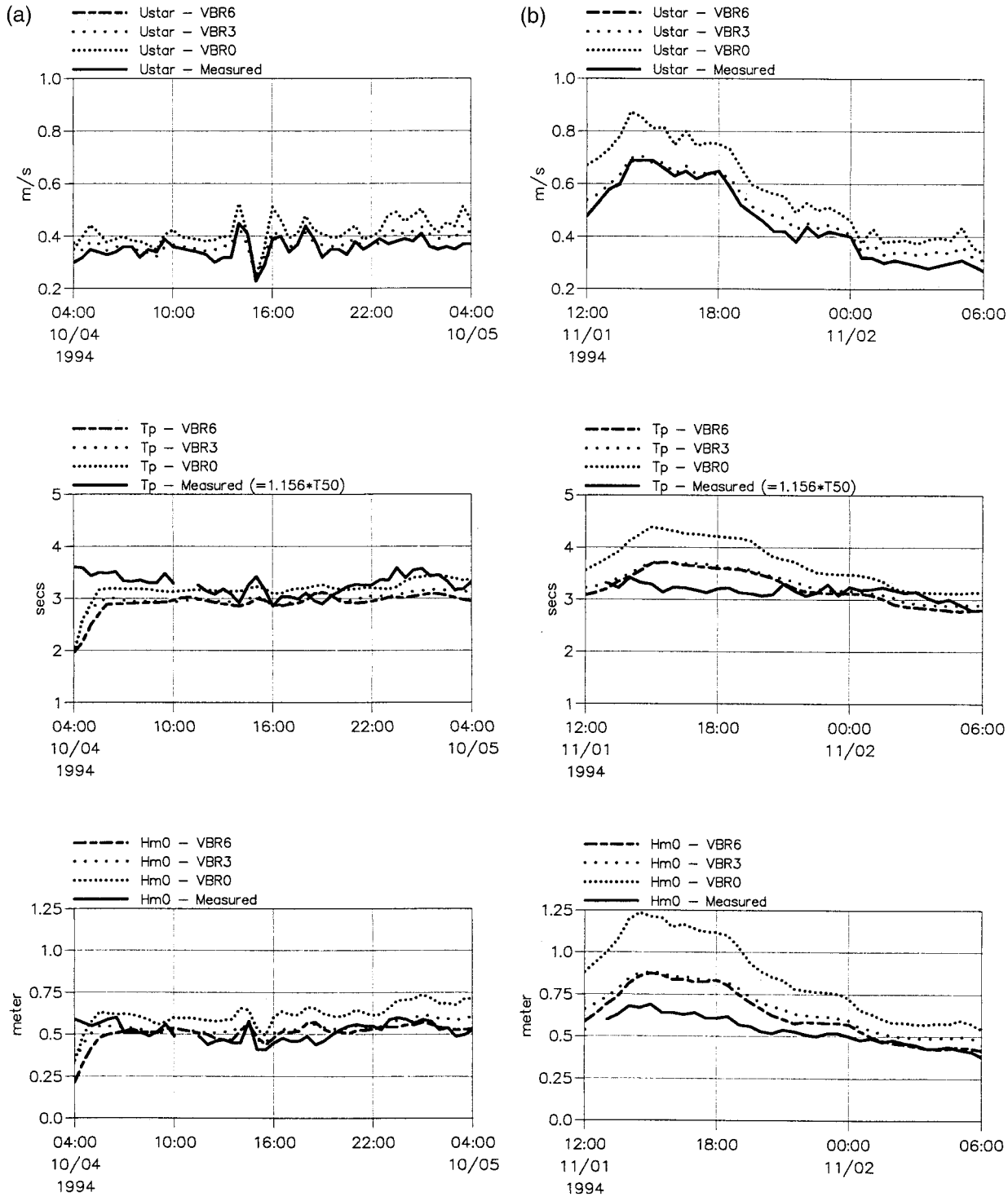

FIG. 10. Comparison between measured data and simulated results using $C_f = 0.0078$ m s^{-1} (a) for event 1 ($U_{10} \sim 10$ m s^{-1}) and (b) for event 2 ($U_{10} \sim 15$ m s^{-1}) (VBR0: standard settings; VBR3: U_{10} input and constant Charnock parameter; VBR6: u_* input and constant Charnock parameter). Upper panel, wind friction velocity; middle panel, peak wave period; and lower panel, significant wave height.

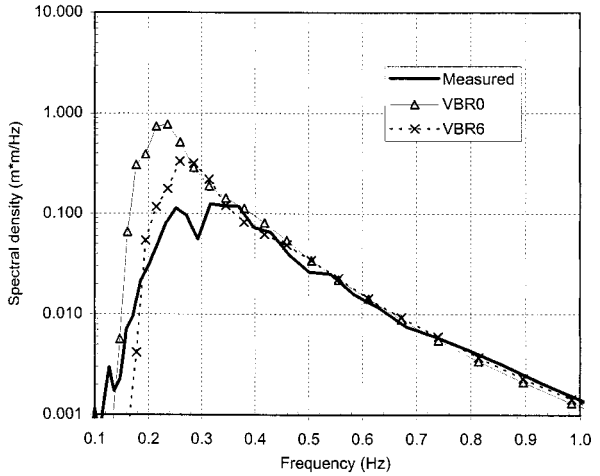

FIG. 11. Comparison between the measured and calculated wave spectra at 1500 LST 1 Nov 1994 for simulations using JONSWAP bottom dissipation coefficient of 0.0078 m s^{-1} (VBR0: U_{10} input, Janssen's sea roughness theory used; VBR6: measured u_* input, Charnock parameter specified as 0.015).

in numerous papers in the past (e.g., Weber 1991; Luo and Monbaliu 1994; Tolman 1994; Komen et al. 1994; Young and Gorman 1995). The present work emphasizes the influence of bottom dissipation on wave age

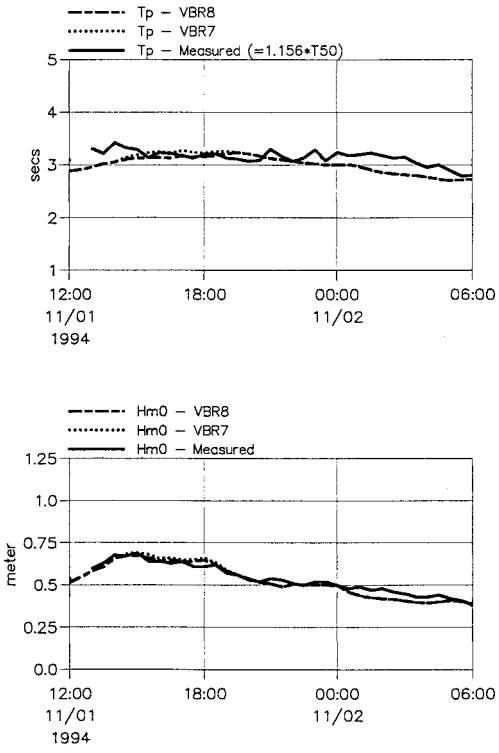

FIG. 12. Comparison between measured and simulated results using measured wind friction speed and different formulations for bottom friction. Upper panel: peak wave period and lower panel: significant wave height. VBR7: CRL (k_N = 0.04 m) and VBR8: MBF (d_{50} = 0.25 mm).

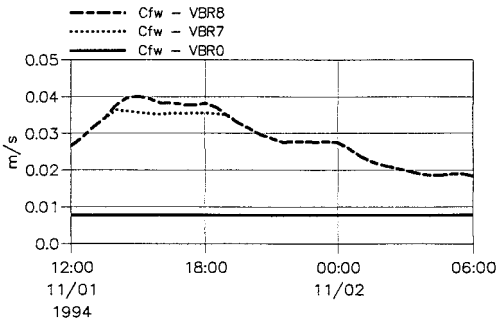

FIG. 13. Temporal variation of the bottom dissipation coefficient for the CRL (simulation VBR7) and MBF (simulation VBR8) bottom friction formulations, and comparison with the JONSWAP value of 0.0078 m s^{-1}.

and sea roughness in a third-generation wind wave model (based on WAM physics) using a wave-dependent sea roughness model (Janssen's model). To the best of our knowledge, this has not been examined before in the present context. The investigation has been based on simple idealized fetch-limited test cases where the water depth is kept constant as well as using a subset of measured data obtained in shallow water (water depth of 4 m) during the RASEX experiment at Vindeby, Denmark.

Three different models for the dissipation coefficient have been considered in the paper. A constant value of the dissipation coefficient as found in the JONSWAP experiment (the JONF model), a model based on a constant geometric roughness length as originally suggested by Weber (1991), the CRL model, and finally a moveable-bed friction model (the MBF model). The latter model is based on the empirical results of Nielsen (1979). He studied wave-formed ripple dimensions in the field caused by irregular waves. The well-know expression for the wave friction factor suggested by Swart

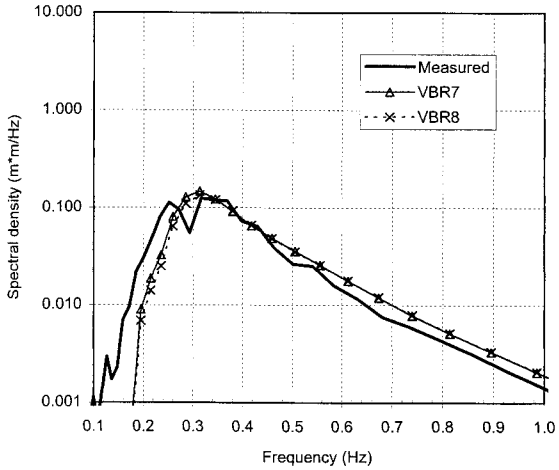

FIG. 14. Comparison between the measured and calculated frequency spectrum at 1500 LST 1 Nov 1994 CRL (simulation VBR7) and MBF (simulation VBR8) bottom friction formulations.

(1974) has been used for the CRL and MBF models. The bottom friction dissipation has been modeled using the linearized bottom friction formulation.

Based on the results of the idealized test cases it was found that the bottom dissipation keep the waves young, which results in increased wind friction. Using the measured wind and wave data from RASEX, it is shown that the Janssen sea roughness parameterization leads to too high sea roughness in shallow water. A constant Charnock parameter of 0.015 was found to perform better for the event with strong winds. In order to obtain good agreement between measured and calculated waves, it was found necessary to use a variable bottom dissipation formulation, where the bottom dissipation coefficient depends in a realistic manner on the hydrodynamic and sediment parameters. The MBF model with $d_{50} = 0.25$ mm gave almost the same results as the CRL model with $k_N = 0.04$ m and are both definite improvement over the JONF model, as have been found elsewhere.

Based on this work, it can be concluded that Janssen's parameterization for sea roughness does not perform well in depth-limited situations. The reason(s) for this is not completely clear. However, we believe it is related to the high values of calculated wave-induced stress τ_w, which is also related to the wind input source term. In cases where bottom dissipation was not important, Janssen et al. (1994) recognized the need to modify the whitecapping dissipation source term (increased the dissipation at high frequencies) in order to get a proper balance between dissipation and Janssen's wind input source term. The imbalance occurs because the wind input scales with $k^{3/2}$ (at high frequencies) while the whitecapping dissipation scales with k. Thus, the wind input will dominate dissipation due to wave breaking, resulting in energy levels which are too high when compared with observations (Janssen et al. 1994). It is speculated that a similar problem occurs in shallow water, possibly with the medium frequency range of the wave spectrum, which is affected by bottom dissipation. As noted in Janssen et al., τ_w is mainly determined by the medium to high frequency range of the wave spectrum. Furthermore, it is possible that the assumed f^{-5} high frequency tail, which is used in the calculation of τ_w (for the frequency range not described in the wave model) is not valid in shallow water. These possibilities were not investigated in this paper.

Acknowledgments. The present work was funded by the Danish Technical Research Council (STVF) and the International Research Centre for Computational Hydrodynamics (ICCH). Their financial support is greatly appreciated. Thanks are due to Messrs Jørgen Højstrup and Søren Larsen, Risø National Laboratory, Denmark, for providing the RASEX data and for their valuable comments. Helpful discussions with Peter Janssen, Hans Jacob Vested, and Per Madsen also influenced this work. The valuable comments, suggestions, and constructive criticism of the anonymous reviewers of the original manuscript are greatly appreciated.

APPENDIX

Calculation of the Wave Friction Factor and Mobile Bed Roughness

a. Wave friction factor

Among the large number of different formulations proposed (see, e.g., Young and Gorman 1995) the implicit expression for the wave friction factor obtained by Jonsson (1966) is here approximated using an explicit expression suggested by Swart (1974):

$$f_w = \begin{cases} \exp\{-5.977 + 5.213(k_N/a_b)^{0.194}\}, & a_{\rm bm}/k_N > 2 \quad \text{(A1a)} \\ 0.24, & a_{\rm bm}/k_N < 2, \quad \text{(A1b)} \end{cases}$$

where $a_{\rm bm}$ $(=U_{\rm bm}/\omega)$ is the amplitude of the orbital excursion. As shown by Young and Gorman, although the various formulations vary quantitatively (particularly for small $a_{\rm bm}/k_N$), they are in qualitative agreement. To avoid confusion please note that the friction coefficient C_f used in Young and Gorman is half of the value used here.

b. Mobile bed roughness

In shallow water, when the orbital velocity penetrates the water depth, the waves exert a shear stress on the sediments at the bed. When the dimensionless shear stress (Shields number θ') is greater than a threshold value (typically 0.05), the waves will move the sediments, and ripples will form. At the other extreme, when the Shields number increases to a very large value (typically 1.0), the ripples will be washed out and the bed becomes flat again. This process has been studied by many investigators in the laboratory and the field (e.g., Inman 1957; Mogridge 1972; Dingler 1974). Basics of ripple formulations can be found in, for example, Weber (1991) and Komen et al. (1994, pp. 156–166).

Based on several field data including irregular waves, Nielsen (1979) proposed the following expression for the geometry of the wave formed ripples:

$$\frac{h_r}{\lambda_r} = \begin{cases} 0.32 \tan\phi, & 0.05 < \theta' < 0.2 \quad \text{(A2a)} \\ 0.342 - 0.34(\theta')^{1/4}, & 0.2 < \theta' < 1 \quad \text{(A2b)} \\ 0, & \theta' > 1, \quad \text{(A2c)} \end{cases}$$

where h_r and λ_r is the ripple height and length, respectively, ϕ is the angle of repose for sand (here taken as 30°), and θ' is the effective dimensionless shear stress calculated using the sand grain roughness, $k_s = 2.5d_{50}$. Here θ' is given by

$$\theta' = \frac{u_*^2}{(s-1)gd_{50}} \quad \text{and} \tag{A3a}$$

$$u_*^2 = \frac{f_w}{2} U_{bm,H_{m0}}^2, \tag{A3b}$$

where $U_{bm,H_{m0}}$ is the maximum orbital velocity at the bed calculated using the significant wave height, H_{m0}. The parameter s is the specific gravity of the bed material.

According to Nielsen, the height of ripples can be obtained by

$$\frac{h_r}{a_{b,H_{m0}}} = 21\Psi^{-1.85} \quad \text{and} \tag{A4a}$$

$$\Psi = \frac{U_{bm,H_{m0}}^2}{(s-1)gD_{50}}, \tag{A4b}$$

where $a_{b,H_{m0}}$ is the amplitude of the orbital excursion at the bed calculated using the significant wave height, H_{m0}. However, using Eqs. (A4) directly leads to unphysical results when $U_{bm,H_{m0}}$ is small. This is largely because the field data on which Eqs. (A4) are based on do not cover such cases. An upper limit for the dimensionless ripple height may be obtained as follows:

$$\left.\frac{h_r}{a_{b,H_{m0}}}\right|_{\max} = \left.\frac{h_r}{\lambda_r}\right|_{\max} \left.\frac{\lambda_r}{a_{b,H_{m0}}}\right|_{\max}. \tag{A5}$$

According to Mogridge (1972), the ripple length cannot exceed the total particle excursion, $2a$. This hypothesis is somewhat confirmed by Nielsen who reported that $\lambda > 2a$ has not been observed in experiments where the orbital excursion was recorded directly. For irregular waves, a is calculated on basis of the significant wave height, H_{m0}. Now using Eq. (A5) (for maximum ripple steepness) and $(\lambda/a_{b,Hm0})_{\max} = 2$, the maximum dimensionless ripple height is given by

$$\left.\frac{h_r}{a_{b,H_{m0}}}\right|_{\max} = 0.64 \tan\phi. \tag{A6}$$

Thus, the dimensionless ripple height is calculated as the minimum value from Eqs. (A5) (A6) as

$$\frac{h_r}{a_{b,H_{m0}}} = \min(21\Psi^{-1.85}, 0.64 \tan\phi), \qquad 0.05 < \theta' < 1. \tag{A7}$$

For $\theta' > 1$, the ripples are washed out ($h_r = 0$) and only skin friction occurs. For extremely large θ' the wave friction increases again due to sheet-flow roughness; see, e.g., Wilson (1989). Our numerical tests showed, however, that this contribution is very small.

The bottom roughness due to ripples is calculated using the following expression suggested by Swart (1976):

$$k_r = 25h_r\frac{h_r}{\lambda_r}. \tag{A8}$$

The empirical relationship is based on a large number of laboratory tests performed with regular (monochromatic) waves. Although it is known that identical geometries may result in different bottom roughness for regular and irregular waves (e.g., Madsen et al. 1990), we use Eq. (A8) in our suggested MBF model for lack of more consistent and general models. Finally the combined ripple and sand grain roughness, k_N, is calculated using

$$k_N = k_r + k_s, \tag{A9}$$

where k_s is the sand grain roughness (skin friction roughness). In the absence of ripples, $k_N = k_s$ as should be expected. Once the combined ripple and sand roughness k_N, is obtained, the wave friction factor f_w is calculated using Eq. (A1) and the dissipation coefficient is calculated using $C_f = f_w U_{\text{bm}}$.

REFERENCES

Barthelmie, R. J., M. S. Courtney, J. Højstrup, and P. Sanderhoff, 1994: The Vindeby Project: A description. Rep. Risø-R-741 (EN), Risø National Laboratory, Roskilde, Denmark, 40 pp. [Available from Risø National Laboratory, P.O. Box 49, DK 4000 Roskilde, Denmark.]

Bouws, E., and G. J. Komen, 1983: On the balance between growth and dissipation in an extreme, depth-limited wind–sea in the southern North Sea. *J. Phys. Oceanogr.,* **13,** 1653–1658.

Brink-Kjaer, O., J. Knudson, G. S. Rodenhuis, and M. Rugbjerg, 1984: Extreme wave conditions in the central North Sea. *Proc. 16th Offshore Technology Conf.,* Houston, TX, 283–293.

Cavaleri, L., and L. H. Holthuijsen, 1998: Wave modelling in the WISE Group. *Proc. 26th Int. Conf. on Coastal Engineering,* Copenhagen, Denmark, ASCE, 498–508.

Charnock, H., 1955: Wind stress on a water surface. *Quart. J. Roy. Meteor. Soc.,* **81,** 639–640.

Collins, J. I., 1972: Prediction of shallow water spectra. *J. Geophys. Res.,* **77,** 2693–2707.

Dingler, J. R., 1974: Wave formed ripples in nearshore sands. Ph.D. thesis, University of California, San Diego, 136 pp.

——, and D. L. Inman, 1976: Wave formed ripples in nearshore sands. *Proc. 15th Int. Conf. on Coastal Engineering,* Honolulu, HI, ASCE, 2109–2126.

Donelan, M. A., F. W. Dobson, S. D. Smith, and R. J. Anderson, 1993: On the dependence of sea surface roughness on wave development. *J. Phys. Oceanogr.,* **23,** 2143–2149.

Graber, H. C., and O. S. Madsen, 1988: A finite-depth wind-wave model. Part 1: Model description. *J. Phys. Oceanogr.,* **18,** 1465–1483.

Günther, H., S. Hasselmann, and P. A. E. M. Janssen, 1992: The WAM model cycle 4. DKRZ Tech. Rep. 4, Hamburg, Germany, 102 pp. [Available from Max Planck Institute for Meteorology, Bundestrasse 56, 20146 Hamburg, Germany.]

Hasselmann, K., 1974: On the spectral dissipation of ocean waves due to whitecapping. *Bound.-Layer Meteor.,* **6,** 107–127.

——, and J. I. Collins, 1968: Spectral dissipation of finite depth gravity waves due to turbulent bottom friction. *J. Mar. Res.,* **26,** 1–12.

Hasselmann, K., and Coauthors, 1973: Measurements of wind–wave growth and swell decay during the Joint North Sea Wave Project (JONSWAP). *Dtsch. Hydrogr.,* **A8** (12), 95 pp.

Hasselmann, S., K. Hasselmann, J. H. Allender, and T. P. Barnett, 1985: Computations and parameterizations of the nonlinear energy transfer in a gravity wave spectrum. Part II: Parameterization of the nonlinear energy transfer for application in wave models. *J. Phys. Oceanogr.,* **15,** 1378–1391.

Hersbach, H., 1998: Application of the adjoint of the WAM model to inverse wave modelling. *J. Geophys. Res.,* **103** (C5), 10 469–10 487.

Inman, D. L., 1957: Wave generated ripples in nearshore sands. Tech. Memo. 100, Beach Erosion Board, U.S. Army Corps of Engineers, 55 pp.

Janssen, P. A. E. M., 1989: Wave induced stress and the drag of airflow over sea waves. *J. Phys. Oceanogr.,* **19,** 745–754.

——, 1991: Quasi-linear theory of wind wave generation applied to wave forecasting. *J. Phys. Oceanogr.,* **21,** 1631–1642.

——, K. Hasselmann, S. Hasselmann, and G. J. Komen, 1994: Parameterisation of source terms and energy balance in a growing wind sea. *Dynamics and Modelling of Ocean Waves,* G. Komen et al., Eds. Cambridge University Press, 215–232.

Johnson, H. K., and H. Kofoed-Hansen, 1998: MIKE21 OSW3G, technical documentation. Internal Rep., Danish Hydraulic Institute, 84 pp.

——, J. Højstrup, H. J. Vested, and S. E. Larsen, 1998: On the Dependence of Sea Surface Roughness on Wind Waves. *J. Phys. Oceanogr.,* **28,** 1702–1716.

——, H. J. Vested, H. Hersbach, J. Højstrup, and S. E. Larsen, 1999: On the coupling between wind and waves in the WAM model. *J. Atmos. Oceanic Technol.,* **16,** 1708–1790.

Jonsson, I. G., 1966: Wave boundary layers and friction factors. *Proc. 10th Int. Conf. on Coastal Engineering,* Tokyo, Japan, ASCE, 127–148.

Kahma, K. K., and C. J. Calkoen, 1994: Growth curve observations. *Dynamics and Modelling of Ocean Waves,* G. Komen et al., Eds. Cambridge University Press, 174–182.

Komen, G. J., L. Cavaleri, M. Donelan, K. Hasselmann, S. Hasselmann, and P. A. E. M. Janssen, 1994: *Dynamics and Modelling of Ocean Waves.* Cambridge University Press, 532 pp.

Luo, W., and J. Monbaliu, 1994: Effects of the bottom friction formulation on the energy balance for gravity waves in shallow water. *J. Geophys. Res.,* **99,** 18 501–18 511.

Madsen, O. S., Y.-K. Poon, and H. C. Graber, 1988: Spectral wave attenuation by bottom friction: Theory. *Proc. 21st Int. Conf. on Coastal Engineering,* Malaga, Spain, ASCE, 492–504.

——, P. P. Mathiesen, and M. M. Rosengaus, 1990: Movable bed friction for spectral waves. *Proc. 22d Int. Conf. on Coastal Engineering,* Delft, Netherlands, ASCE, 420–429.

Mogridge, G. R., 1972: Wave generated bed forms. Ph.D. thesis, Queens University, Kingston, ON, Canada, 246 pp.

Nielsen, P., 1979: Some basic concepts of wave sediment transport. Series Paper 20, Institute of Hydrodynamic and Hydraulic Engineering, Technical University of Denmark, 160 pp.

——, 1983: Analytical determination of nearshore wave height variation due to refraction, shoaling and friction. *Coastal Eng.,* **7,** 233–251.

Plant, W. J., 1982: A relation between wind stress and wave slope. *J. Geophys. Res.,* **87** (C), 1961–1967.

Shemdin, O., K. Hasselmann, S. V. Hsiao, and K. Heterich, 1978: Nonlinear and linear bottom interaction effects in shallow water. *Turbulent Fluxes through the Sea Surface, Wave Dynamics and Prediction,* A. Farve and K. Hasselmann, Eds., Plenum Press, 347–372.

Smith, S. D., and Coauthors, 1992: Sea surface wind stress and drag coefficients: The HEXOS results. *Bound.-Layer Meteor.,* **60,** 109–142.

Swart, D. H., 1974: Offshore sediment transport and equilibrium beach profiles. Delft Hydraulics Laboratory Publ. No. 131, 302 pp.

——, 1976: Predictive equations regarding coastal transports. *Proc. 15th Int. Conf. on Coastal Engineering,* Honolulu, HI, ASCE, 1113–1132.

Tolman, H. L., 1994: Wind-waves and moveable bed bottom friction. *J. Phys. Oceanogr.,* **24,** 994–1009.

The WAMDI Group, S. J. 1988: The WAM model—A third generation ocean wave prediction model. *J. Phys. Oceanogr.,* **18,** 1775–1810.

Weber, S. L., 1988: The energy balance of finite depth gravity waves. *J. Geophys. Res.,* **93** (C4), 3601–3607.

——, 1991: Bottom friction for wind sea and swell in extreme depth-limited situations. *J. Phys. Oceanogr.,* **21,** 149–172.

Wilson, K. C., 1989: Friction of wave-induced sheet flow. *Coastal Eng.,* **12,** 371–379.

Wu, J., 1980: Wind stress coefficients over sea surface near neutral conditions. A revisit. *J. Phys. Oceanogr.,* **10,** 727–740.

Young, I., and R. M. Gorman, 1995: Measurements of the evolution of ocean wave spectra due to bottom friction. *J. Geophys. Res.,* **100** (C6), 10 987–11 004.